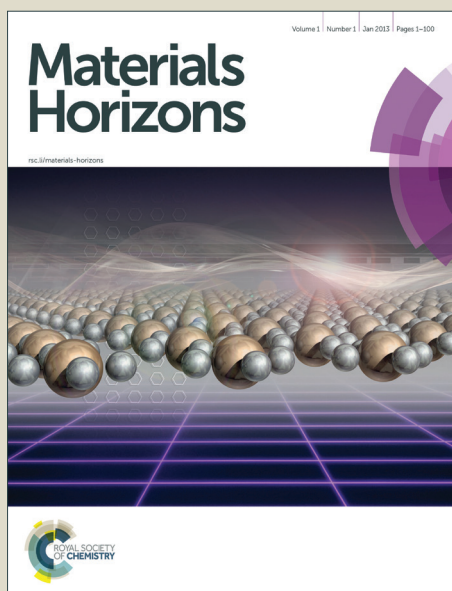


Materials Horizons

Accepted Manuscript



This is an *Accepted Manuscript*, which has been through the Royal Society of Chemistry peer review process and has been accepted for publication.

Accepted Manuscripts are published online shortly after acceptance, before technical editing, formatting and proof reading. Using this free service, authors can make their results available to the community, in citable form, before we publish the edited article. We will replace this *Accepted Manuscript* with the edited and formatted *Advance Article* as soon as it is available.

You can find more information about *Accepted Manuscripts* in the [Information for Authors](#).

Please note that technical editing may introduce minor changes to the text and/or graphics, which may alter content. The journal's standard [Terms & Conditions](#) and the [Ethical guidelines](#) still apply. In no event shall the Royal Society of Chemistry be held responsible for any errors or omissions in this *Accepted Manuscript* or any consequences arising from the use of any information it contains.



COMMUNICATION

Simultaneous Spin-Coating and Solvent Annealing: Manipulating the Active Layer Morphology to a Power Conversion Efficiency of 9.6% in Polymer Solar Cells

Received 00th January 20xx,
Accepted 00th January 20xx

DOI: 10.1039/x0xx00000x

www.rsc.org/

Zhicai He,¹ Feng Liu,^{2, 3, †} Cheng Wang,⁴ Jihua Chen,⁵ Lilin He,⁶ Dennis Nordlund,⁷ Hongbin Wu,^{1, †} Thomas P. Russell,^{2, 3, 8, †} and Yong Cao¹

We developed a simultaneous spin-coating/solvent-annealing process and demonstrate the morphology optimization for PTB7 based organic photovoltaics. This novel processing method enhances the edge-on crystalline content in the thin films and induces the formation of weak PCBM aggregates. As a result, the efficiency of polymer solar cells increased from 9.2% to a certified high efficiency of 9.61%, owing to an enhanced short-circuit current (J_{sc} , 18.4 mA cm⁻² vs. 17.5 mA cm⁻²) and improved fill factor.

In the past decade, the performance of polymer-based bulk heterojunction (BHJ) organic photovoltaics (OPV) has increased tremendously, from 5% to ~10%.^{1,2} Given the advances in the synthesis of photoactive polymers,³ further improvement of device performance requires understanding and controlling the kinetically-trapped morphologies of polymer-based BHJ OPVs so that the size scale of phase separation can be fine-tuned.^{4,5} This requires understanding and controlling the thermodynamics, e.g. polymer/solvent, polymer/small molecule and polymer/additive interactions, and the interplay of multiple kinetic processes, e.g. solvent evaporation, polymer aggregation and ordering, inter-diffusion, and phase separation. When coupled with the development of new materials, further rapid growth in OPV

performance can be expected. The synthesis of novel light absorbing polymers, like poly[[4,8-bis[(2-ethylhexyl)oxy]benzo[1,2-b:4,5-b']dithiophene-2,6-diyl][3-fluoro-2-[(2-ethylhexyl)carbonyl]thieno[3,4-b]thiophenediyl]] (PTB7)⁶⁻⁹ (structure shown in Supporting Information), is one example, exhibiting power conversion efficiencies (PCEs) > 9%.² PTB7 has a deep highest occupied molecular orbital (HOMO) energy level, which helps to increase the open circuit voltage (V_{oc}) of the resultant solar cell devices. Solution-cast thin films of PTB7 show a "face-on" crystal orientation, although the crystallinity is low.¹⁰ OPV devices based on PTB7 characteristically have a large short circuit current (J_{sc}), resulting from the small length scale of the phase separated morphology.¹¹⁻¹³ The use of a processing additive, like 8-diiodooctane (DIO), has been essential to control the size scale of the morphology.¹¹⁻¹³ Device parameters, like a 70% fill factor and 17.46 mA/cm² current density, have established milestone records.² To further enhance performance, it is evident that novel processing strategies must be developed that tailor the thermodynamics and kinetics associated with the phase separation of the components. Solvent vapor annealing method has been used to optimize the morphology of the active layer in polymer light-emitting diodes,¹⁴ organic thin film transistors,¹⁵ and polymer solar cells.^{16,17} Here we introduced a new annealing process to prepare BHJ active layer films where the rate of solvent evaporation and, hence, interactions between the PTB7 and PCBM, are controlled. This enables control of the ultimate size scale of the phase-separated morphology and the orientation of components within the active layer and the generation of active layer morphologies with high PCEs.

Thin films of PTB7 and PCBM mixtures were spin coated in a closed environment to reduce the rate of solvent evaporation and, simultaneously, solvent annealed the film, as shown schematically in Scheme S1 (Supporting Information). This controlled solvent evaporation influences the ability of the PTB7 to order and, therefore, the morphology of the BHJ active layer.^{18,19} When coupling this controlled solvent evaporation (1,2-dichlorobenzene, DCB) with an additive (3 vol% 1,8-diiodooctane, DIO), devices with highly reproducible PCEs of 9.77% can be achieved.

¹ Institute of Polymer Optoelectronic Materials and Devices, State Key Laboratory of Luminescent Materials and Devices, South China University of Technology, Guangzhou 510640, P. R. China. Email: hbwu@scut.edu.cn

² Materials Sciences Division, Lawrence Berkeley National Lab, Berkeley, California, 94720, United States. Email: iamfengliu@gmail.com

³ Dept of Polymer Science and Engineering, University of Massachusetts, Amherst, Massachusetts 01003, United States. Email: russell@mail.pse.umass.edu

⁴ Advanced Light Source, Lawrence Berkeley National Lab, Berkeley, California, 94720, United States

⁵ Center for Nanophase Materials Sciences, Oak Ridge National Laboratory, Oak Ridge, Tennessee 37831, United States

⁶ Biology and Soft Matter Division, Neutron Sciences Directorate, Oak Ridge National Laboratory, Oak Ridge, TN 37831, USA

⁷ Stanford Synchrotron Radiation Lightsource, SLAC National Accelerator Laboratory, Menlo Park, California 94025, United States

⁸ WPI-Advanced Institute for Materials Research, Tohoku University, 2-1-1 Katahira, Aoba, Sendai 980-8577, Japan.

† Electronic Supplementary Information (ESI) available. See DOI: 10.1039/x0xx00000x

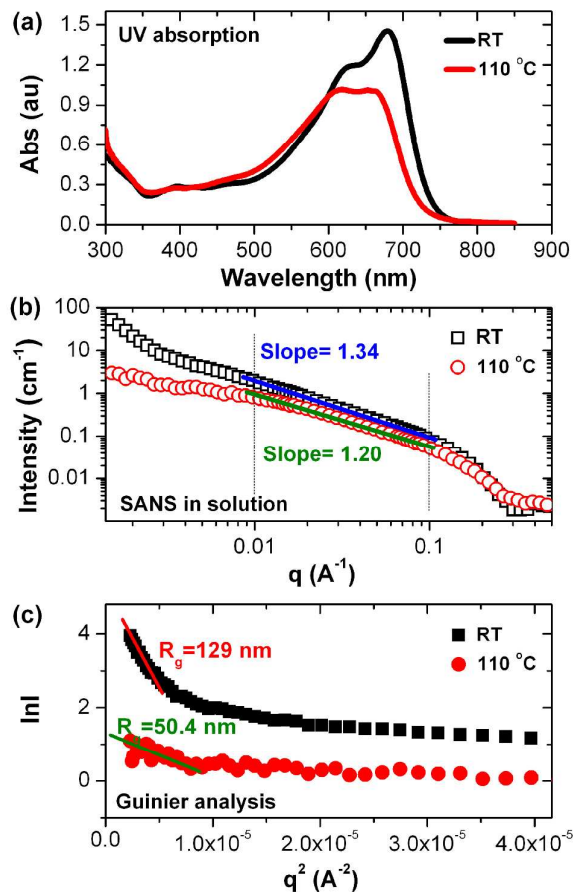


Figure 1. (a) UV-vis absorption and (b) small angle neutron scattering of PTB7 in deuterated DCB solutions; (c) Guinier analysis of small angle neutron scattering result.

BHJ thin film morphology is strongly dependent on the solvent removal rate and the state of the polymer in solution. We first characterized the polymer chain in solution using absorption and scattering methods to probe the electronic coupling and structure.²⁰ Shown in Figure 1a are the room temperature and 110 °C UV-vis absorption spectra of dilute solutions of PTB7 in DCB (~1mg/ml). At 25 °C, the absorption spectrum of PTB7 shows a sharp peak at 680 nm and a shoulder at 625 nm. By increasing the solution temperature to 110 °C, an obvious decrease in the long wavelength peak is seen along with a blue-shift to 658 nm. Similarly, the shoulder at 625 nm is blue-shifted to 617 nm. These results suggest that, at room temperature, the PTB7 chains are not isolated from each other but, rather, exhibit a tendency to form J-aggregates²¹, leading to an electronic coupling between the chains. Molecular aggregation was probed by small angle neutron scattering (SANS) using 10mg/ml deuterated 1,2-dichlorobenzene solutions. The 25 °C and 110 °C transmission scattering profiles are shown in Figure 1b. The scattering profiles at both temperatures are quite similar in the high q region. However, at the low temperature a rapid upturn in the scattering at low q is seen, indicative of aggregation. The scattering data (Figure 1b), plotted in a log-log manner as a function

of q, show very different behavior in different scattering vector ranges. For $q < \sim 0.007 \text{ \AA}^{-1}$, a distinct upturn in the scattering is evident. For $0.01 \text{ \AA}^{-1} < q < \sim 0.1 \text{ \AA}^{-1}$, the scattering follows a power law behavior. At higher q, a dramatic reduction in the scattering for higher q is observed. A Guinier analysis was used to analyze the scattering at low q (Figure 1c),^{22,23} from which the scattering could be described by entities having radii of gyration, R_g , of ~129 nm for the PTB7 solution at 25 °C. Guinier-Porod fitting in the low q region gives an R_g of 114 nm and a Porod exponent of 3.4.^{24,25} A Guinier-Porod fitting in the higher q range resulted in an R_g of 25 nm and a Porod exponent of 1.17. By heating the solution to 110 °C, the R_g describing the lowest q data decreased to ~50 nm (Guinier analysis), while at slightly higher q, an R_g of ~26 nm and Porod exponent of 1.15 were found (Guinier-Porod fitting). The intensity of the scattering at low q increased markedly for the solutions at 25 °C, indicating the formation of large aggregates with high mass as the temperature decreased.

Prior to spin coating the active layer, a thin layer of poly[(9,9-bis(3'-(N,N-dimethylamino)propyl)-2,7-fluorene)-alt-2,7-(9,9-dioctylfluorene)] (PFN) with a thickness of ~10 nm was coated onto the ITO, which reduces the work function of ITO to ~ -4.1 eV, making it suitable for the fabrication of inverted devices.² The orientation of the PFN chains at the ITO surface was probed by near edge x-ray absorption fine structure (NEXAFS) analysis,⁵ taking advantage of the polarized nature of synchrotron radiation.²⁶ The NEXAFS spectra the PFN film, taken at various incidence angles with respect to the surface plane, is shown in Figure S2 (Supporting Information). They show a prominent absorption edge at 285.4 eV that corresponds to the C=C π^* resonance of the aromatic backbone. We observe that the cross-section of the π^* resonance is strongest at grazing incidence (e-vector out-of-plane) and weakest at normal incidence (e-vector in-plane), whereas the C=C σ^* states (at higher energy) display the opposite behaviour. Although the angular dependence is not so prominent, it indicates that the aromatic backbone of PFN assume a face-on orientation tendency, which is advantageous for charge transport and collection at the cathode. A schematic illustration of PFN chains and orientation of the side chain functional group are shown in Figure S2 (Supporting Information). The interaction of the functional side chains lowers the ITO work function while the planarized backbone serves as an electron conductor and hole blocking layer, due to its low lying HOMO energy level.

A 25 mg/ml solution of PTB7:PCBM blends in 1,2-dichlorobenzene with 3 v % additives was heated to 60 °C for 2h before use. The active layer solution was deposited onto the substrate mounted onto a spin head in a closed chamber. After the solution was dropped atop of the substrate, the chamber was closed and the spin coater was turned on rapidly. The spin coating and solvent annealing treatment were done simultaneously, and the duration is 1 minute. The film was then removed and vacuum dried at room temperature overnight to remove residual solvent and additives. Subsequently, MoO₃ (10nm) and Ag (100 nm) were thermally evaporated onto the active layer to complete the device. Devices prepared in this manner showed PCEs up to 9.77% (results summarized in Table 1, the statistic results counted over 18 individual devices can be seen in Table S2). The current density of

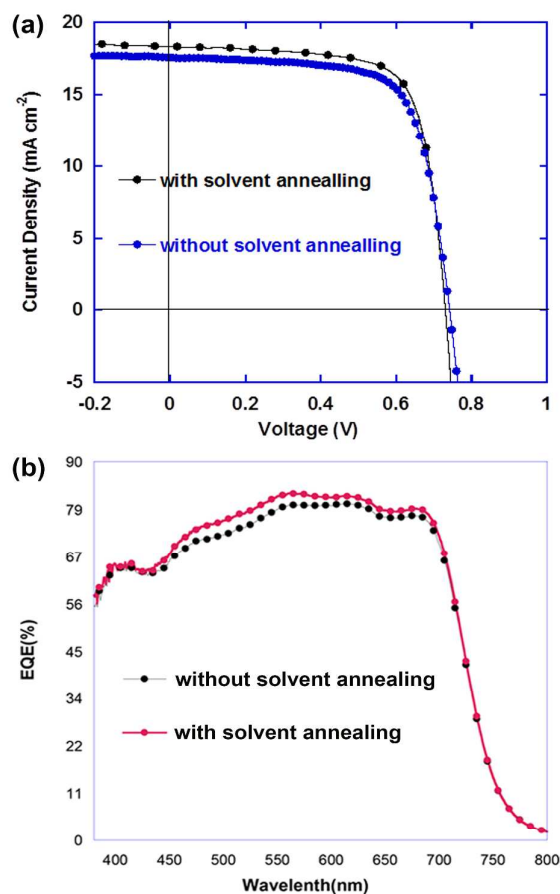


Figure 2. Device performance comparison fabricated by using conventional and new spin coating methods.

Table 1. PTB7:PCBM solar cells performances

Device	PCE (%)	J_{sc} (mA/cm ²)	FF (%)	V_{oc} (V)
Without annealing	9.24	17.54	71.00	0.742
With annealing	9.77	18.28	73.36	0.730

the devices reached 18.28 mA/cm² and the fill factor (FF) reached 73% (Figure 2a).

Devices processed using normal spin coating method showed efficiencies of ~9.24%. It is also worthy of mentioning that the widely used solvent annealing treatment after spin coating lead to a slight decrease in performance (9.02% PCE, with a V_{oc} = 0.80 V, J_{sc} = 15.2 mA/cm², and FF = 67.7%. See Table S1 in Supporting Information for detail). The major factors contributing to the enhanced PCE were the increases in the current density and fill factor, which strongly correlated to the morphology of the BHJ film.

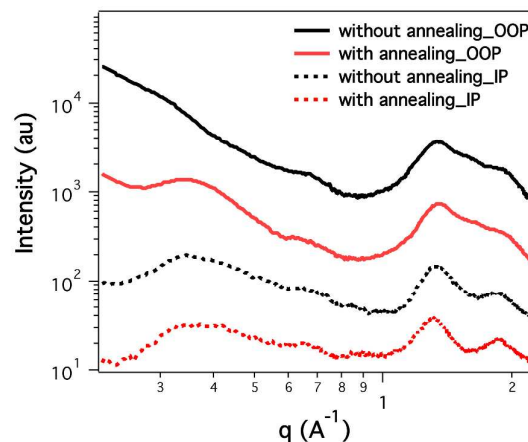


Figure 3. GIXD of BHJ thin films processed by using conventional and new spin coating methods. OOP: out-of-plane; IP: in-plane.

The EQE of the solvent annealed devices also increased from 450 to 700 nm, in a region both PTB7 and PCBM contributes, in keeping with the increase in J_{sc} (Figure 2b). The best-performing device was then sealed and certified by the National Centre of Supervision and Inspection on Solar Photovoltaic Products Quality of China (CPVT) where the device was characterized with a PCE of 9.61% (with a J_{sc} of 18.43 mA/cm² and a FF of 69%), which is obviously higher than our previous record of 9.214%,² representing a new record high certified efficiency for single-layer BHJ devices based on PTB7 (Supporting Information).

The morphologies of the active layers with and without solvent annealing were characterized to understand the origin of the performance enhancement. Shown in Figure 3 are the in-plane and out-of-plane grazing incidence diffraction (GIXD) profiles of PTB7:PCBM thin films processed using conventional and the new spin coating methods. In the out-of-plane data of the conventional spin coated film, the alkyl-to-alkyl lamellae stacking peak is quite weak. Yet, in the corresponding in-plane region, a broad (100) peak is seen at 0.33 Å⁻¹, corresponding to the inter-chain separation distance of 19.0 Å. This result indicates that the PTB7 polymer assume a face-on orientation. An intense diffraction peak is seen at 1.34 Å⁻¹ arising from the PCBM (with a relative peak area of 219.5 au). Multi-peak fitting was used to analyze the diffraction in this region (details shown in the Supporting Information). A weak reflection at 1.63 Å⁻¹ corresponds to the $\pi\pi$ stacking (relative peak area of 34.0 au). For the solvent annealing processed thin film, a more pronounced (100) peak is seen in the out-of-plane direction, indicating that more edge-on oriented crystals exist in this sample. Analyzing the high q region, we find that the PCBM peak shows a slightly enhance peak area of 229 au. The $\pi\pi$ stacking peak area is 58.8 au and the full width at half maximum of 0.22 Å⁻¹. It is evident that spin coating with solvent annealing promotes the crystallization of the PTB7, which could be an important contribution to the performance improvement in the devices. In GIXD, a stronger edge-on orientation of the solvent annealed BHJ thin film is seen, and it is shown that edge-on oriented crystallites

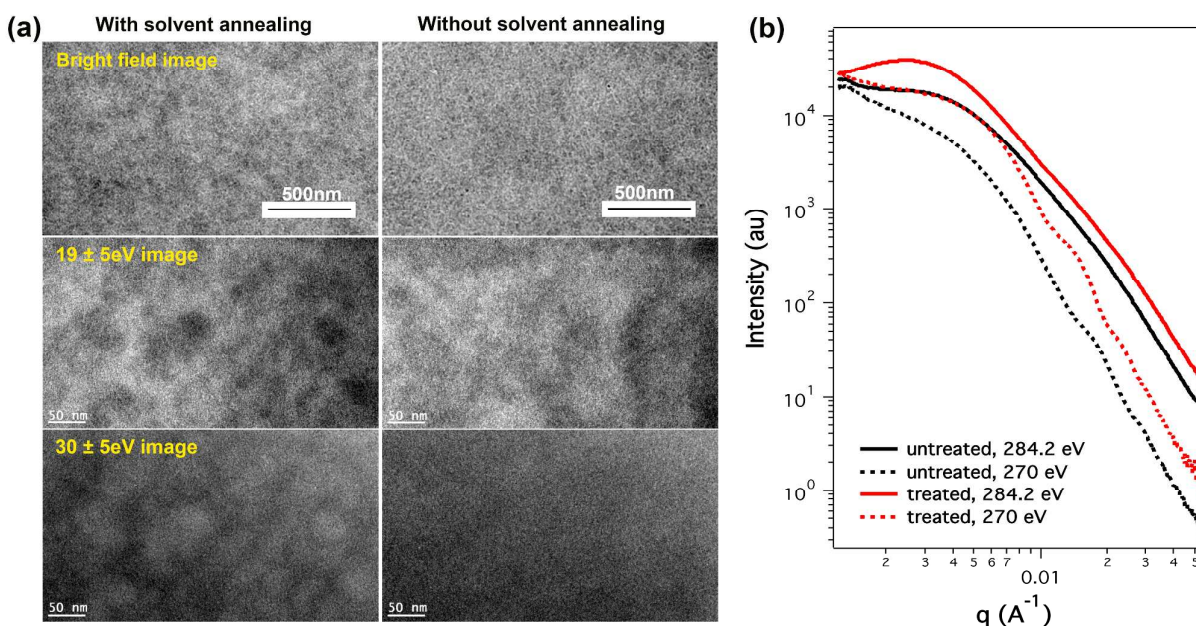


Figure 4. (a) TEM characterization of PTB7:PCBM BHJ thin films casted from conventional and new spin coating methods. Top row: bright field TEM; second row: 19 eV image; third row: 30 eV image. (b) Resonant soft x-ray scattering of BHJ thin films processed from conventional spin coating and new spin coating methods.

can form nano-sized fibrils (Figure 4a and Supporting Information), which, in turn, establishes a prominent network structure to function better in devices.

Bright field and energy filtered transmission electron micrographs (TEM) of BHJ samples are shown in Figure 4a (The contrast is a function of both thickness and composition). Conventional spin coated active layer thin films give rise to a fibrillar network structure (See Supporting Information for enlarged images). Under solvent annealing conditions, the bright field TEM image showed stronger density fluctuations and kept in a fibrillar type of morphology. The slightly darker areas, that are irregular in size and shape, are PCBM aggregates, showing an inter-distance of hundreds of nanometers. These PCBM aggregates are weak and the film density fluctuation is low compared to none additive processed PTB7:PCBM blends, in which high purity PCBM aggregations dominate the morphology.⁶ In current case those aggregates are PCBM enrichment areas, which still contains large amount of PTB7. The fibrillar network structure is prominent within the film, thus a high J_{sc} is maintained. The comparison of these two films indicates that slight PCBM aggregation is not deleterious to the performance of OPV BHJs, since a smooth film can be obtained under the conditions used without gradients in the composition of the components. In energy filtered TEM, energy window at 19 eV was used to image PTB7 and 30 eV to image PCBM.²⁷ The PTB7 map and PCBM map showed complementary images, suggesting a compositional variation in the thin films. The color variation in these images corresponds to the PCBM aggregations inside the film, supporting the results obtained by bright field TEM. It should also be noted that in the thickness map of the energy filtered TEM images, the color variation is similar to that in energy filtered TEM

images, which is quite evident in the solvent annealed sample (Figure 4a and Supporting Information). The concurrence of thickness variation and phase separation suggests that phase separation could be an important factor for their irregular shaped top surface morphology (Figure S7). It also explains the similarity of the low q region in the scattering characterizations.

The characteristic length scales of the phase separated morphology in the BHJ thin film is another critical factor that determines the performance of devices. This aspect was studied by complementary scattering and microscopy methods. Shown in Figure 4b is the resonant soft x-ray scattering (RSOXS) of PTB7:PCBM thin films prepared under the two spin coating procedures.²⁸ In the experiments, 284.2 eV (carbon K-edge) photon energy was used to probe the morphology, while 270 eV (off edge) photon energy was used to probe the thickness variation of the thin film.¹¹ The conventional spin coated sample shows a maximum in the intensity at $q \sim 0.004 \text{ \AA}^{-1}$ for a 284.2 eV photon energy, corresponding to a characteristic length scale of 157 nm. A similar length scale has previously been observed in several studies, indicating a large scaled phase separation in BHJ thin films, though the exact origin is still being questioned.¹¹⁻¹³ The high q region in the RSOXS profile decays slowly, which masks the interferences arising from other length scales of phase separation ($\sim 0.02 \text{ \AA}^{-1}$), defining a much finer phase separation that is commensurate with exciton diffusion length, promoting a high PCE in PTB7:PCBM blends. For photon energies less than 270 eV, a shoulder at $\sim 0.004 \text{ \AA}^{-1}$ is observed, attributed to the thickness variations in the thin film.¹¹ The spin coating with solvent annealing shows a different RSOXS profile in the low q region. An obvious scattering peak at 0.0025 \AA^{-1} is observed, which corresponds to a characteristic length scale of 250

nm. This interference can be associated with weak PCBM aggregations, as observed by TEM. Similarly, interferences at higher scattering vectors are observed, corresponding to a finer morphology that is associated with a high photon-current in devices. At 270 eV photon-energy, the scattering profile of the solvent annealed sample showed a higher intensity compared to samples prepared with conventional spin coating, indicating a rougher surface. The dual length scale observed in BHJ thin films is an interesting phenomenon, though it is hard to directly correlate to device performance. It is evident from the neutron scattering results, multiple lengths scales of aggregation is observed in PTB7 solutions that, more than likely, serve as precursors to the multi-length scale morphology observed in the solid active layer that gives rise to improved performance.

In conclusion, we have developed a new device fabrication method for polymer solar cells that shows enhanced device performance. The morphological details of the resultant active layer were thoroughly investigated with numerous structural probes. It is shown that spin coating with a solvent annealing procedure enhances the edge-on crystalline content in the active layer and increases PCBM aggregations. The new procedure results in enhanced film roughness and large featured domains, which came from the different drying process.

Acknowledgements

H.W. and Z. H acknowledge financial support from the National Nature Science Foundation of China (nos91333206, 51403066, 51225301, 61177022 and 5141101251), Fundamental Research Funds for the Central Universities (2014ZM001) and Innovation Program of Guangdong Province Universities and Colleges (2012KJCX0009), and thank M. Yun and X. Wang of CPVT for device performance verification. F.L. and T.P.R. were supported by Polymer-Based Materials for Harvesting Solar Energy (PHaSE), an Energy Frontier Research Centre funded by the U.S. Department of Energy, Office of Basic Energy Sciences under award number DE-SC0001087. Portions of this research were carried out at beamline 7.3.3 and 11.0.1.2 at the Advanced Light Source, and Molecular Foundry, Lawrence Berkeley National Laboratory, which was supported by the DOE, Office of Science, and Office of Basic Energy Sciences. Use of the Stanford Synchrotron Radiation Light source, SLAC National Accelerator Laboratory, is supported by the U.S. Department of Energy, Office of Science, Office of Basic Energy Sciences under Contract No. DE-AC02-76SF00515. Energy filtered TEM was conducted at the Center for Nanophase Materials Sciences, which is sponsored at Oak Ridge National Laboratory by the Division of Scientific User Facilities, Office of Basic Energy Sciences, U.S. Department of Energy. Research conducted at ORNL's High Flux Isotope Reactor was sponsored by the Scientific User Facilities Division, Office of Basic Energy Sciences, US Department of Energy.

Notes and references

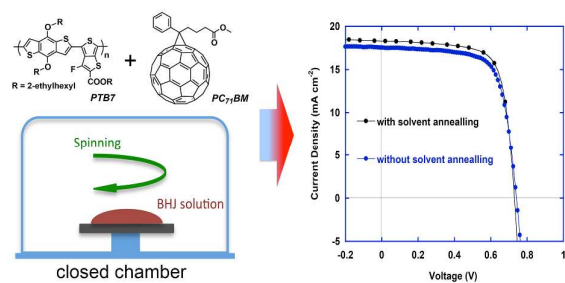
1. J. You, L. Dou, K. Yoshimura, T. Kato, K. Ohya, T. Moriarty, K. Emery, C.-C. Chen, J. Gao, G. Li, and Y. Yang, *Nat. Commun.*,

- 2013, **4**, 1446 p1–10.
2. Z. He, C. Zhong, S. Su, M. Xu, H. Wu, and Y. Cao, *Nat. Photon.*, 2012, **6**, 593–597.
3. L. Bian, E. Zhu, J. Tang, W. Tang, and F. Zhang, *Prog. Polym. Sci.*, 2012, **37**, 1292–1331.
4. F. Liu, Y. Gu, J. W. Jung, W. H. Jo, and T. P. Russell, *J. Polym. Sci., Part B: Polym. Phys.*, 2012, **50**, 1018–1044.
5. F. Liu, Y. Gu, X. Shen, S. Ferdous, H.-W. Wang, and T. P. Russell, *Prog. Polym. Sci.*, 2013, **38**, 1990–2052.
6. Y. Liang, Z. Xu, J. Xia, S.-T. Tsai, Y. Wu, G. Li, C. Ray, and L. Yu, *Adv. Mater.*, 2010, **22**, E135–E138.
7. Y. Liang, D. Feng, Y. Wu, S.-T. Tsai, G. Li, C. Ray, and L. Yu, *J. Am. Chem. Soc.*, 2009, **131**, 7792–7799.
8. H. J. Son, W. Wang, T. Xu, Y. Liang, Y. Wu, G. Li, and L. Yu, *J. Am. Chem. Soc.*, 2011, **133**, 1885–1894.
9. H.-Y. Chen, J. Hou, S. Zhang, Y. Liang, G. Yang, Y. Yang, L. Yu, Y. Wu, and G. Li, *Nat. Photon.*, 2009, **3**, 649–653.
10. M. R. Hammond, R. J. Kline, A. A. Herzing, L. J. Richter, D. S. Germack, H.-W. Ro, C. L. Soles, D. A. Fischer, T. Xu, L. Yu, M. F. Toney, and D. M. DeLongchamp, *ACS Nano*, 2011, **5**, 8248–8257.
11. B. A. Collins, Z. Li, J. R. Tumbleston, E. Gann, C. R. McNeill, and H. Ade, *Adv. Energy Mater.*, 2013, **3**, 65–74.
12. F. Liu, Z. Wei, J. R. Tumbleston, C. Wang, Y. Gu, D. Wang, A. L. Briseno, H. Ade, and T. P. Russell, *Adv. Energy Mater.*, 2014, **4**, 1301377.
13. W. Chen, T. Xu, F. He, W. Wang, C. Wang, J. Strzalka, Y. Liu, J. Wen, D. J. Miller, J. Chen, K. Hong, L. Yu, and S. B. Darling, *Nano Lett.*, 2011, **11**, 3707–3713.
14. B. Yao, B. Zhang, J. Ding, Z. Xie, J. Zhang, and L. Wang, *Org. Electron.*, 2013, **14**, 897–901.
15. H. Chang, P. Wang, H. Li, J. Zhang, and D. Yan, *Synth. Met.*, 2013, **184**, 1–4.
16. Y. Kim, S. A. Choulis, J. Nelson, D. D. C. Bradley, S. Cook, and J. R. Durrant, *Appl. Phys. Lett.*, 2005, **86**, 063502 p1–3.
17. J. J. van Franeker, M. Turbiez, W. Li, M. M. Wienk, and R. E. A. J. Janssen, *Nat. Commun.*, 2015, **6**, 1–8.
18. G. Li, Y. Yao, H. Yang, V. Shrotriya, G. Yang, and Y. Yang, *Adv. Funct. Mater.*, 2007, **17**, 1636–1644.
19. G. Li, V. Shrotriya, J. Huang, Y. Yao, T. Moriarty, E. Keith, and Y. Yang, *Nat. Mater.*, 2005, **4**, 864–868.
20. K. Schmidt, C. J. Tassone, J. R. Niskala, A. T. Yiu, O. P. Lee, T. M. Weiss, C. Wang, J. M. J. Fréchet, P. M. Beaujuge, and M. F. Toney, *Adv. Mater.*, 2013, **26**, 300–305.
21. J. Clark, C. Silva, R. H. Friend, and F. C. Spano, *Phys. Rev. Lett.*, 2007, **98**, 206406 p1–4.
22. M.-Y. Chiu, U.-S. Jeng, C.-H. Su, K. S. Liang, and K.-H. Wei, *Adv. Mater.*, 2008, **20**, 2573–2578.
23. D. Chen, A. Nakahara, D. Wei, D. Nordlund, and T. P. Russell, *Nano Lett.*, 2011, **11**, 561–567.
24. G. Beaucage, *J Appl Crystal.*, 1996, **29**, 134–146.
25. G. Beaucage, *J Appl Crystal.*, 1995, 1–12.
26. J. Park, R. Yang, C. V. Hoven, A. Garcia, D. A. Fischer, T.-Q. Nguyen, G. C. Bazan, and D. M. DeLongchamp, *Adv. Mater.*, 2008, **20**, 2491–2496.
27. L. F. Drummy, R. J. Davis, D. L. Moore, M. Durstock, R. A. Vaia, and J. W. P. Hsu, *Chem. Mater.*, 2011, **23**, 907–912.
28. E. Gann, A. T. Young, B. A. Collins, H. Yan, J. Nasiatka, H. A. Padmore, H. Ade, A. Hexemer, and C. Wang, *Rev. Sci. Instrum.*, 2012, **83**, 045110.

Toc Graphic

COMMUNICATION

Journal Name



We demonstrate spin coating in together with solvent annealing can be used to tune the morphology of BHJ active layer and thus enhance device performances.

Conceptual Insights Statement

Polymer solar cells (PSCs) is an emerging photovoltaic technology, which have attracted enormous attention and gaining more and more tremendous importance since they have already been proven to be a promising, renewable, lightweight and low-cost energy source. In spite of the great enthusiasm about PSCs in recent years, their performance, especially the power conversion efficiency (PCE) remains low, which restrict their practical use.

In the present work we developed a novel bulk heterojunction thin film preparation method for polymer solar cells (PSCs) that uses a solvent vapor annealing during the spin-coating process and observed a marked device performance enhancement to a very high efficiency of 9.77% (certified at 9.61%). Detailed grazing x-ray diffraction, resonant soft x-ray scattering and energy filtered transmission electron microscopy showed that the solvent vapor annealing changed the polymer crystallization, PCBM aggregation, and the extent of phase separation. Neutron scattering was used to probe the single chain behavior, uncovering a multi-length scaled aggregation of the conjugated polymer that depended on temperature. This correlated with the multi-length scale morphology in PSCs thin films. The studies demonstrate a fundamental advance in the structure property relationship in PSCs that it will be beneficial to the community of organic electronics.

The work reported here further provide an important step toward the realization of economical solar cells with high efficiency comparable to that of the best amorphous/microcrystalline Si solar cells or the best organic tandem cells yet reported, representing a key advance towards a new efficiency regime for PSCs. Therefore, we expect more and more PSCs will enter the next regime with efficiency of 10-11% when this method is applied to many other active emerging donor materials with a starting efficiency of about 5-8%).